High-resolution computed tomography with a compact soft x-ray microscope

Michael Bertilson*, Olov von Hofsten, Ulrich Vogt, Anders Holmberg, and Hans M. Hertz

Biomedical & X-Ray Physics, Department of Applied Physics, Royal Institute of Technology/AlbaNova, SE-106 91 Stockholm, Sweden

**Corresponding author: michael.bertilson@biox.kth.se*

Abstract: Computed tomography based on high-resolution soft x-ray microscopy utilizes the natural contrast for biological specimens provided by the water window ($\lambda = 2.4$ - 4.4 nm) and the high resolving power of zone plate objectives. It is capable of revealing the 3D structure of biological specimens at sub-visible-microscopic resolution. To date, the technique has only been available at synchrotron-based microscopes, which limits the researchers access. In the present paper we demonstrate high-resolution soft x-ray tomography with a laboratory zone-plate-based soft x-ray microscope. The specimen, a diatom mounted on a glass capillary, was reconstructed from a tilt series of 53 images covering 180º using a filtered back projection algorithm. The resolution of the tomogram was estimated to a half period of 140 nm using a differential-phase-residual method. Cryo-fixation, increased source brightness and extended-depth-of-focus objectives are important for pushing the resolution of compact systems for biological samples.

OCIS codes: (180.7460) X-ray microscopy; (110.6955) Tomographic imaging; (260.6048) Soft x-rays; (340.0340) X-ray optics

References and links

1. J. B. Pawley, *Handbook of biological confocal microscopy*, 3rd edition (Springer Science+Business Media, LLC, 2006).
2. W. Chao, B. D. Harteneck, J. A. Liddle, E. H. Anderson, and D. Attwood, "Soft X-ray microscopy at a spatial resolution better than 15 nm," Nature **435**, 1210-1213 (2005).
3. D. Weiss, G. Schneider, B. Niemann, P Guttman, D. Rudolph, and G. Schmahl, "Computed tomography of cryogenic biological specimens based on X-ray microscopic images," Ultramicroscopy. **84**, 185-197 (2000).
4. D. Attwood, *Soft x-rays and extreme ultraviolet radiation: Principles and Applications*, (Cambridge University Press, 2007).
5. M. Berglund, L. Rymell, M. Peuker, T. Wilhein, and H. M. Hertz, "Compact water-window transmission X-ray microscopy," J. Microsc. **197**, 268-273 (2000).
6. P. A. C. Takman, H. Stollberg, G. A. Johansson, A. Holmberg, M. Lindblom, and H. M. Hertz, "High-resolution compact X-ray microscopy," J. Microsc. **226**, 175 (2007).
7. M. Bertilson, O. von Hofsten, J. Thieme, M. Lindblom, A. Holmberg, P. Takman, U. Vogt, and H. M. Hertz, "First application experiments with the Stockholm compact soft x-ray microscope" presented at the 9th international conference on x-ray microscopy, Zürich, Switzerland, 21-25 July 2008.
8. M. Benk, K. Bergmann, D. Schäfer, and T. Wilhein, "Compact soft x-ray microscope using a gas-discharge light source," Opt. Lett. **33**, 2359-2361 (2008)
9. M. Hoshino and S. Aoki, "Laboratory-scale soft X-ray imaging microtomography using Wolter mirror optics," Appl. Phys. Expr. **1**, 067005 (2008).
10. J. Lehr, "3D X-ray microscopy: tomographic imaging of mineral sheaths of bacteria Leptothrix Ochracea with the Gottingen X-ray microscope at BESSY," Optik **104**, 166 (1997).
11. C. A. Larabell and M. A. Le Gros, "X-ray tomography generates 3-D reconstructions fo the yeast, Saccharomyces cerevisiae, at 60-nm resolution," Mol. Biol. Cell. **15**, 957-962 (2004).
12. D. Y. Parkinson, G. McDermott, L. D. Etkin, M. A. Le Gros and C. A. Larabell, "Quantitative 3-D imaging of eukaryotic cells using soft X-ray tomography," J. Struct. Biol. **162**, 380-386 (2008).

#107683 - $15.00 USD Received 17 Feb 2009; revised 21 Apr 2009; accepted 10 Jun 2009; published 18 Jun 2009

13. A. Tkachuk, M. Feser, H. Cui, F. Duewer, H Chang, and W. Yun, Xradia, Inc. "High-resolution x-ray tomography using laboratory sources," Proc. SPIE **6318**, 1-8 (2006), http://www.xradia.com.
14. J. de Groot, O. Hemberg, A. Holmberg, and H. M. Hertz, "Target optimization of a water-window liquid-jet laser-plasma source," J. Appl. Phys. **94**, 3717 (2003).
15. H. Stollberg, S. Yulin, P. A. C. Takman, and H. M. Hertz, "High-reflectivity Cr/Sc multilayer condenser for compact water-window microscopy," Rev. Sci. Instrum. **77**, 123101 (2006).
16. A. Holmberg, S. Rehbein, and H. M. Hertz, "Nano-fabrication of condenser and micro zone plates for compact x-ray microscopy," Microelectron. Eng., **73-74**, 639 (2004).
17. J. R. Kremer, D. N. Mastronarde, and R. McIntosh, "Computer visualization of three-dimensional image data using IMOD," J. Struct. Biol. **116**, 71-76 (1996). [http://bio3d.colorado.edu/imod/].
18. J. Frank, *Three-dimensional electron microscopy of macromolecular assemblies,* (Oxford university press, 2006).
19. A. C. Kak and M. Slaney, *Principles of computerized tomographic imaging*, IEEE Press (1988).
20. Amira®, Visage Imaging, http://www.visageimaging.com.
21. D. Wiess, G. Schneider, S. Vogt, P. Guttmann, B. Niemann, D. Rudolph, and G. Schmahl, "Tomographic imaging of biological specimens with the cryo transmission x-ray microscope," NIMPR A **467-468**, 1308-1311 (2001).
22. A. Sakdinawat, Y. Liu, D. Attwood, W. Chao, and E. Andersson, "Specialized diffractive optics for contrast and resolution enhancement" presented at the 9th international conference on x-ray microscopy, Zürich, Switzerland, 21-25 July 2008.

1. Introduction

Three-dimensional microscopic imaging is gaining importance in several research areas, for instance in cell biology. Presently such imaging is primarily based on confocal visible-light microscopy [1] with its typical lateral diffraction-limited resolution of approximately 250 nm. Soft x-ray microscopy in the water window ($\lambda = 2.4 - 4.4$ nm) offers 10 times higher resolution when it is based on zone-plate optics [2]. Computed tomography based on soft x-ray microscopy images can therefore be used for reconstructing the three-dimensional (3D) inner structure of specimens with high resolution [3]. The technique was demonstrated, and is only available, at synchrotron-based x-ray microscopes. The access to these large facilities is, however, limited and many researchers would benefit from having this imaging technique available in their own laboratory. In the present paper we therefore demonstrate high-resolution soft x-ray tomography performed with a laboratory zone-plate based water-window x-ray microscope.

Two-dimensional (2D) soft x-ray microscopy in the water window is an emerging technique for nanometer-resolution imaging in cell biology. The method utilizes the natural contrast mechanism between protein and water in the water window, offers deep penetration, ~10 μm in aqueous samples, and combines it with the high resolving power of diffractive zone plate objectives [4]. The Rayleigh resolution r of a zone plate objective, used in the first diffraction order, is limited by its outermost zone width Δr according to $r = 1.22\Delta r$. So far, line widths (half periods) down to 15 nm have been resolved using zone plates [2]. Zone plate based soft x-ray microscopy is therefore capable of imaging unsliced and hydrated samples at a resolution of tens of nanometer without extensive sample preparation. However, most soft x-ray microscopes rely on high brightness synchrotron radiation sources, which result in limited access to the technique for external researchers. For this reason we developed the first compact soft x-ray microscope with a liquid-jet laser-plasma source [5]. The new generation of this microscope features operation at either $\lambda = 3.37$ nm or $\lambda = 2.48$ nm and images wet or dry samples in stereo with a resolution better than 30 nm half periods [6,7]. Other compact soft x-ray microscope systems are based on discharge sources [8], which results in longer exposure times, or uses objectives based on reflective optics giving lower resolution [9].

The negligible refraction of soft x-rays in the sample and the relatively long depth of focus (DOF), in the order of microns, of zone plate objectives make soft x-ray microscopy suitable for 3D tomographic imaging, analogous to computed tomography in medical imaging [3]. Three-dimensional microscopic imaging in the water-window was first demonstrated by Haddad *et al.* who used a scanning microscope to image a gold test sample [10]. The technique was improved for biological samples when cryo fixation, which reduces the

#107683 - $15.00 USD Received 17 Feb 2009; revised 21 Apr 2009; accepted 10 Jun 2009; published 18 Jun 2009

radiation damage, was introduced [3]. Larabell and LeGros have since then refined the technique for high-throughput cell studies [11]. Data for high-quality tomograms of biological samples can today be routinely acquired in a few minutes on a synchrotron soft x-ray microscope [12].

In the present paper we demonstrate high-resolution tomography performed with a laboratory soft x-ray microscope. The system is based on a laser-plasma source for quasi-monochromatic illumination allowing the use of 30 nm zone plate objectives for high-resolution imaging. Previous work in laboratory high-resolution tomography includes a commercial zone-plate-based system for hard x-ray 3D imaging for non-biological applications [13] and a lower-resolution system based on Wolter optics and a broad-band laser-plasma source operating in the water window [9]. Finally it should be noted that tomography based on transmission electron microscopy (TEM) allows for very-high-resolution laboratory 3D imaging. However, these techniques involve time consuming sample preparation and is limited to < 500 nm thin specimens [11], which is not the case for soft x-ray microscopy.

2. Experimental arrangement

Figure 1 shows the experimental arrangement, which is based on the $\lambda = 3.37$ nm operation mode of the Stockholm compact soft x-ray microscope [7]. This wavelength was chosen since it results in a somewhat shorter exposure time for dry samples compared to operation at $\lambda = 2.48$ nm.

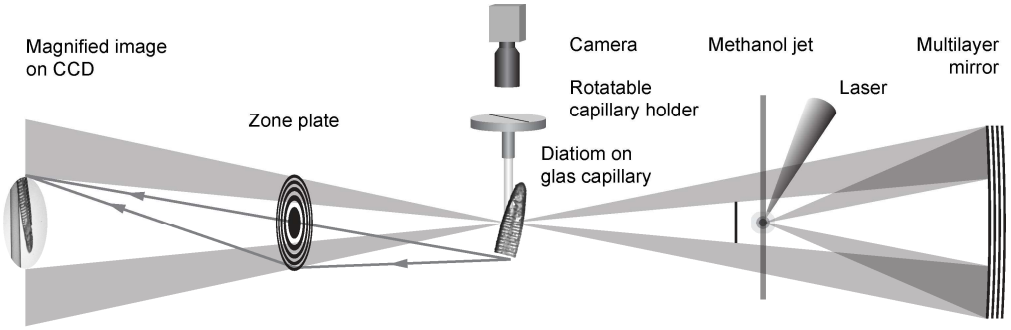

Fig. 1. Illustration showing the arrangement of the microscope.

The soft x-ray emitting plasma is generated with a pulsed high-power laser beam ($\lambda = 532$ nm, ~3 ns, 100 Hz, ~100 mJ), which is focused onto the laminar part of a liquid methanol jet. This results in a photon flux of $\sim 5 \cdot 10^{13}$ photons/(s×sr) at $\lambda = 3.37$ nm [14] with an emission line monochromaticity of $\lambda/\Delta\lambda > 500$. The source then illuminates the sample with a numerical aperture of 0.063 via critical illumination employing a normal-incidence Cr/Sc multilayer condenser mirror [15]. The mirror acts as a monochromator, selecting the $\lambda = 3.37$ nm peak from the source. Laser light scattered from the source is blocked by a 300 nm titanium filter. A central stop, between the plasma and the sample, blocks direct illumination in the central part of the detector, creating a field of view (FOV) of ~16 μm in the sample plane. The average photon flux incident on the sample in this area is about $\sim 2 \cdot 10^{6}$ photons/(s×μm^2).

A 360° rotatable glass capillary sample holder, kept at atmospheric pressure, allows projection series of both hydrated and dry samples to be acquired. The tilt angle of the sample holder is monitored with a telescope-equipped video camera aimed down the rotation axis of the holder.

The sample is imaged onto a soft x-ray sensitive back-illuminated thinned CCD detector (16 bit, 13.5 μm × 13.5 μm pixels size, 2048 × 2048 pixels) using an in-house fabricated [16] nickel zone plate objective with an outermost zone width $\Delta r = 30$ nm and focal length

#107683 - $15.00 USD Received 17 Feb 2009; revised 21 Apr 2009; accepted 10 Jun 2009; published 18 Jun 2009

500 μm. The numerical aperture (NA) of this zone plate is almost matched to the NA of the illumination, which makes the optical system photon efficient. Under these conditions the DOF for diffraction limited performance is limited to $DOF = 4\Delta r^2 \cdot \lambda^{-1} \approx 1$ μm. A larger sample depth can however be accepted for less strict resolution requirements.

3. Method

Fossil diatoms are three-dimensional structures mainly consisting of silicon dioxide with features on the nano-to-micrometer scale. The attenuation length of silicon dioxide (~400 nm @ $\lambda = 3.37$ nm) gives them good contrast while still being transparent, which makes them suitable as test samples for high-resolution computed tomography. A thin and hollow fossil diatom with an outer diameter of 2.0 – 4.2 μm was therefore selected for the experiment.

The 3D structure of the diatom was imaged using computed tomography, which reconstructs the inner structure of a sample from a set of projections. The imaging method will be described in three steps, starting with the acquisition of the tilt series, followed by image alignment and image corrections, and ending with the tomographic reconstruction.

3.1. Data acquisition

The diatom was mounted at the fine tip of a glass capillary, which then was placed in the rotatable capillary holder. The imaging magnification was selected to 1230 giving a pixel size of 11 nm in the sample plane. This corresponds to an oversampling by a factor of 1.7 compared to the diffraction-limited Rayleigh resolution of the zone plate objective. The diatom was then imaged from 53 unique tilt angles in the interval 0° – 180°. Each image was acquired with an exposure time of 120 s to make sure that a sufficient signal was detected even through the most absorbing areas of the diatom. Figure 2(a) shows a typical unprocessed image from the tilt series. The angle is increased manually by direct rotation of the capillary holder. Together with the feedback given from the telescope-equipped video camera the estimated accuracy of the manual rotation is about 1°. Snap shots of the rotation stage are recorded for each tilt angle so that the actual tilt angle can be determined with higher accuracy. After each rotation the sample must be brought back to the center of FOV. For refocusing the sample again, several exposures may be necessary. This makes refocusing one of the most time consuming parts of the acquisition process. Adding time for manual adjustments and the exposure time, results in an acquisition rate of about 10 images/h.

3.2. Image processing & alignment

Before the images can be used for the reconstruction they must be aligned with a common axis of rotation and the tilt angles must be known. Computed tomography is ideally based on theoretical parallel projections, not magnified images obtained in a microscope. The differences cause inaccuracies in the reconstruction and the noise make segmentation and later quantitative analysis more difficult. Corrections are therefore made for background signal, inhomogeneous illumination, illumination fluctuations and noise. The reduced modulation of higher spatial frequencies caused by the zone-plate objective [3] can, in principle, be corrected for, but it has not been done here.

The tilt angles are determined by analyzing the snap shot images of the sample holder. The tilt angle increment in this experiment deviated from its average of 3.36° with a standard deviation of 0.9°. This deviation should however not create any major artifacts since each angle is known with an estimated accuracy smaller than ±0.1°.

The alignment of the projection images is done in Midas (a tool for manual alignment based on visual comparisons of projection images), which is a part of the free tomography program package IMOD [17]. The alignment was made by tracking features in the sample and by centering the capillary visually. A set of transformations was then calculated for moving the common axis of rotation to the center of the diatom instead. This way the projections can be cropped tighter around the sample, reducing the amount of data to be processed in the reconstruction.

#107683 - $15.00 USD Received 17 Feb 2009; revised 21 Apr 2009; accepted 10 Jun 2009; published 18 Jun 2009

The inhomogeneous illumination, seen in Fig. 2(a), is a direct result of the critical illumination. The radiation source is directly imaged onto the sample resulting in a Gaussian-like illumination profile. To compensate for this a Gaussian function is fitted to the illumination in the image by adjusting its position, widths and rotation angle. The resulting function is then used for the correction. Fig. 2(b) demonstrates the result. The contrast in the upper left inserts of Figs. 2(a) and 2(b) has been increased to more clearly demonstrate the difference between the original and the corrected image.

Image noise was reduced using wavelet coefficient thresholding. The projection images were decomposed with a multilevel 2D stationary wavelet transformation based on the Haar wavelet. A threshold giving sufficient noise reduction was then applied to the wavelet coefficients before reconstructing the image using the inverse wavelet transform. Figures 2(a) and 2(b) shows a typical projection image before and after noise reduction, respectively. The lower inserts in Figs. 2(a) and 2(b) show an enlarged area of the sample to demonstrate the improvement.

Finally, the illumination of the image series is normalized and the areas outside the field-of-view are replaced by extrapolating the illumination.

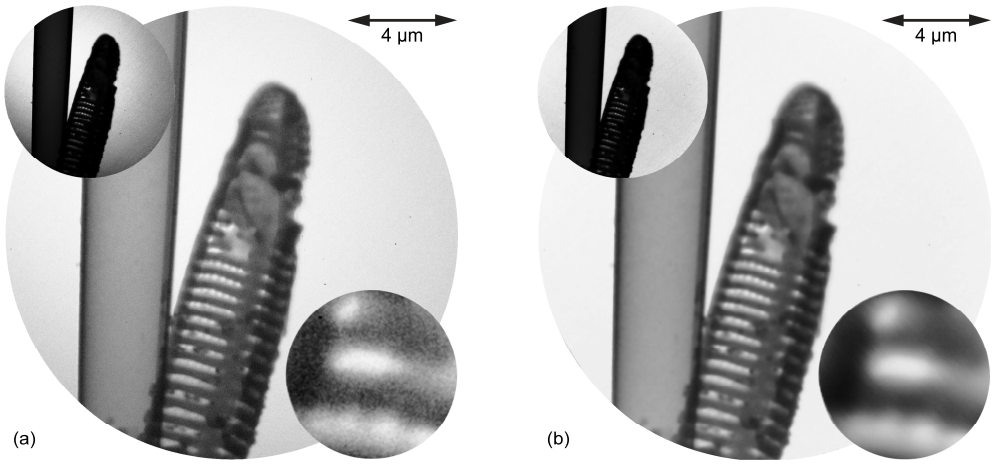

Fig. 2. (a) shows an original projection image, whereas (b) shows the same projection image after denoising and illumination correction. The inserts have been added to more clearly demonstrate the improvements.

3.3. Tomographic reconstruction

To reduce the amount of computer memory and computer power needed for the reconstruction the already aligned and corrected projections were subsampled and cropped around the centered diatom. The resolution of the reconstruction was not expected to be diffraction limited. Due to defocus blur and uncertainties in the visual alignment the estimated half-period resolution in the axial direction of the reconstruction is approximately ~40 nm. Moreover, the Crowther resolution, $r_c = \Delta\theta \cdot D$, specifies the smallest period r_c, which can be consistently reconstructed from projections of a sample with diameter D and tilt angle increments of $\Delta\theta$ [18]. According to this criterion, the estimated half period resolution in the reconstruction planes is about 130 nm. This indicates heavy oversampling in the direction orthogonal to the axis of rotation. The projections could therefore be scaled down 4 times, resulting in 44 nm square pixels, without loosing resolution in the reconstructed sections. The reconstruction presented in this paper was done with a filtered back projection (FBP) algorithm [19]. To reduce the sharp artifacts and increased high-frequency noise caused by the standard ramp filter a Hann window filter was also applied. The reconstructed volume, which consist of $300 \times 300 \times 328$ cubic 44 nm voxels was reconstructed in about 5 minutes on a standard personal computer.

#107683 - $15.00 USD Received 17 Feb 2009; revised 21 Apr 2009; accepted 10 Jun 2009; published 18 Jun 2009

4. Results and discussion

The reconstruction is demonstrated in Figs. 3(a) – 3(f), where gray-scaled slices from different angles through the tomogram are shown. The dark and bright areas represent low and high sample transmissions respectively. Figure 3(a) shows a section orthogonal to the axis of rotation where the capillary and the upper area of the diatom can be seen. Figures 3(b) and 3(c) clearly show the edge of the big diatom opening and some structures inside the diatom. Figure 3(d) shows a section through the upper area of the diatom whereas Figs. 3(e) and 3(f) are from the central area. These sections show that the small grating-like openings are resolved in the middle as well as the top region. The average half-period of this pattern is less than 150 nm.

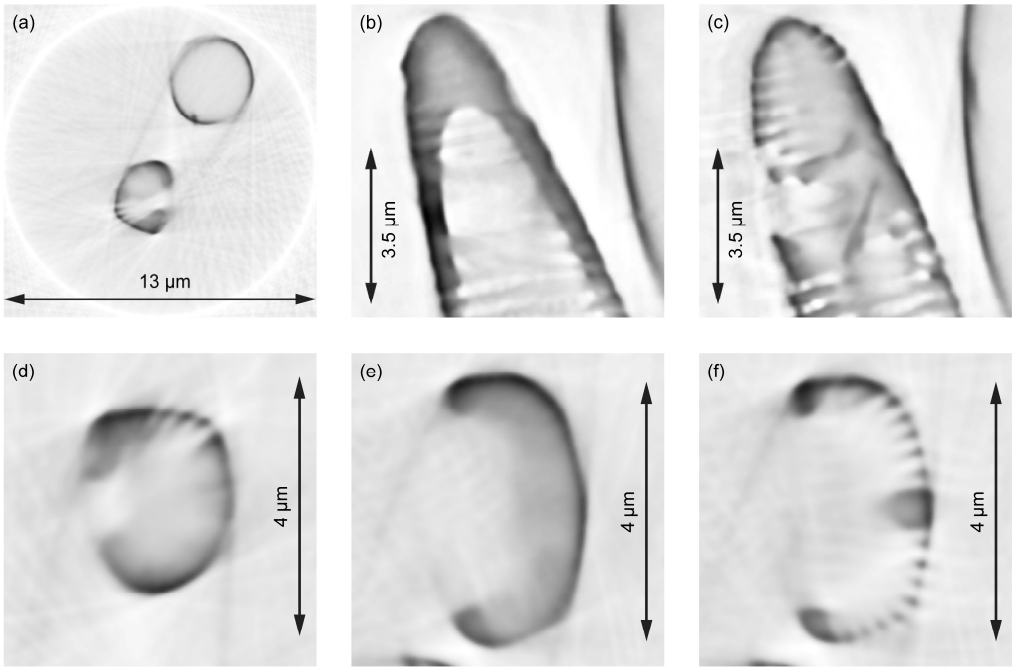

Fig. 3. Selected slices through the reconstructed tomgram showing the structure of the diatom. (a) shows a section of the whole reconstructed region, (b) and (c) are slizes showing the large diatom opening and some internal structures, (d-f) show slizes through the diatom in which the small grating-like structure of the diatom is resolved.

Today, reconstructed tomograms can easily be visualized and analyzed using existing software on standards personal computers. To demonstrate one of many ways to visualize the reconstructions to the reader, a rotation series of the diatom is shown in Fig. 4. The visualization has been done with Amira® [20], using a technique where the intensity and transparency of each voxel depend on the value of the corresponding voxel in the reconstruction. The capillary has been hidden to more clearly show the structure of the diatom. Two animations of the reconstructed diatom (Media 1, Media 2) are provided in the online version of the paper, of which one is stereo color-coded (Media 2). When viewed through correctly color-filtered goggles a 3D impression of the diatom can be experienced.

#107683 - $15.00 USD Received 17 Feb 2009; revised 21 Apr 2009; accepted 10 Jun 2009; published 18 Jun 2009

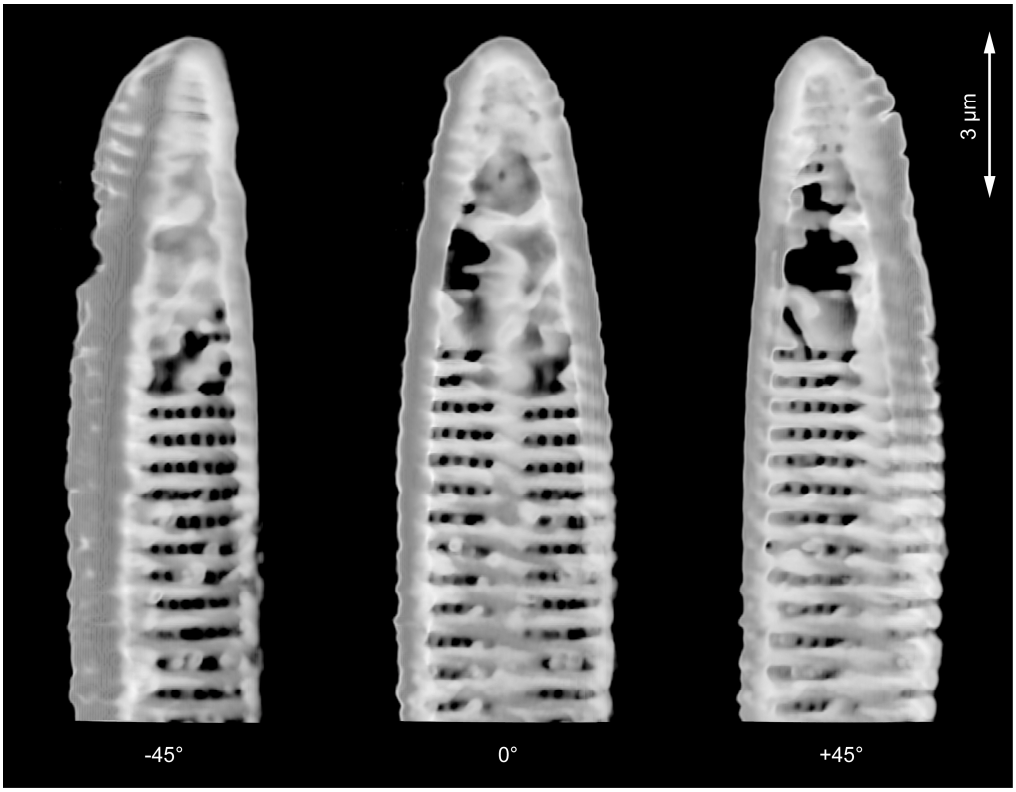

Fig. 4. Rotation series of the reconstructed diatom. The capillary has been removed to show the internal structure. Animations are available online (Media 1), (Media 2).

The resolution of reconstructed sections can be estimated by analyzing the differential phase residual (DPR), $\Delta\varphi(\nu,\Delta\nu)$ [19, 21], where ν is the spatial frequency and $\Delta\nu$ a frequency interval. The DPR compares the Fourier transform of two independent reconstructions of the same sample and measures the root mean square of the phase difference, weighted by the average amplitude. A low DPR indicates good correlation between the two reconstructions, for that spatial frequency. As the correlation decreases, the DPR will approach 90° (the average of a totally random phase difference). Figure 5 presents the sectional average DPR in the central diatom region, calculated from reconstructions based on the odd and even projections respectively, as a function of spatial frequency ν ($\Delta\nu = 0.27$). The DPR analysis was limited to the diatom structure and its close surroundings by multiplying the reconstructed sections with a mask prior to the DPR analysis. The influence of the masks edges on the calculated DPR was limited to low spatial frequencies by convolving a binary mask with a broad (600 nm full width at half maximum) Gaussian function. The dashed curve in Fig. 5 shows the DPR when the same mask is applied to sections of random noise. The softened edges of the mask clearly cause phase correlations for low frequencies, up to ~2 μm^{-1}, but leaves higher frequencies unaffected. The spatial frequency ν_{45} for which the DPR rises above 45° is used as a criterion for resolution in reconstructed images [19]. When this criterion is applied to the DPR curve in Fig. 5, the resolution is estimated to 3.6 μm^{-1}, which corresponds to a half period of 140 nm. In the section with the highest resolution, the corresponding resolution is 132 nm.

#107683 - $15.00 USD Received 17 Feb 2009; revised 21 Apr 2009; accepted 10 Jun 2009; published 18 Jun 2009

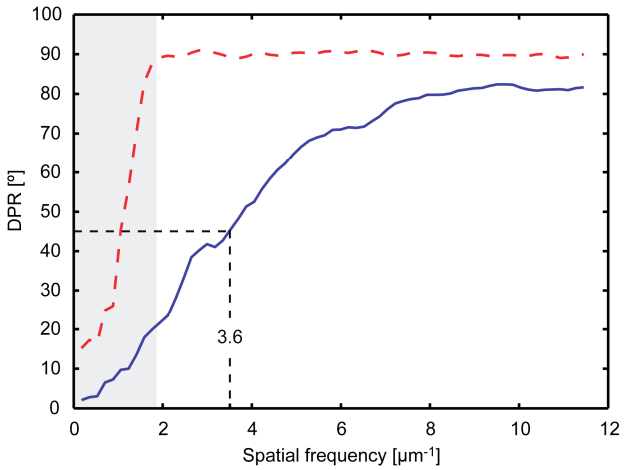

Fig. 5. The sectional average differential phase residual (DPR) calculated between two equally masked but independently reconstructed regions of the diatom. The dashed line shows the DPR when the same mask was applied to random noise.

The resolution analysis agrees with the resolution estimated from observing the details in the diatom shown in Fig. 3(f). The capillary however, was defocused in many of the projections, which results in lower contrast and blurring in the corresponding directions of the reconstruction (cf. Fig. 3(a)). To some degree these artifacts are seen in the diatom as well. However, the analysis show that the overall achieved resolution in the diatom was close to the Crowther criteria, which indicates that neither the small DOF nor the visual alignment did reduce the resolution significantly.

It is important to note that the tomographic resolution demonstrated in this paper was not limited by the resolution of the zone plate objective. Improved resolution can be obtained by increasing the number of projections as long as the DOF can be matched to the sample thickness. This is easily done for thin samples. But increasing the resolution for thicker samples, in the order of a few microns thick, without sacrificing too much precious illumination, is more complicated. This is because the DOF depends on the outer zone width Δr of the zone plate, which also determines its NA. An outer zone width of $\Delta r = 50$ nm would, for example, give a DOF of ~3 μm, but on the other hand it would loose 80% of the direct illumination due to the mismatch of NAs. Such a loss would have a large impact on the total acquisition time for a full tilt series. It would also result in an unnecessary radiation dose being deposited in sample.

There are alternative ways to extend the DOF of zone plates of which one is to reduce the monochromaticity of the illumination [8]. The strong chromaticity of the zone plate then creates an extended DOF at the cost of lower modulation for higher spatial frequencies. This, however, is only possible if the monochromaticity of the source is controllable. This makes the development of diffractive optics that combine high NAs with an extended DOF, like cubic phase plate zone plates [22], of particular interest for compact soft x-ray microscopy.

As mentioned earlier an increased number of projections are also required for improving the resolution. Here the source brightness and the penetration depth become important, especially for hydrated samples. The attenuation length of $\lambda = 2.48$ nm is longer than for $\lambda = 3.37$ nm, which becomes important when studying biological specimens and soils in their natural hydrated environment. The $\lambda = 2.48$ nm wavelength also provides a larger DOF and a more relaxed working distance which is convenient when rotating the sample. Increasing the source brightness and efficiency of the condenser optics for the $\lambda = 2.48$ nm operation mode is therefore of interest for pushing the resolution and usability of computed tomography based on compact soft x-ray microscopy.

#107683 - $15.00 USD Received 17 Feb 2009; revised 21 Apr 2009; accepted 10 Jun 2009; published 18 Jun 2009

5. Conclusions and Outlook

We have demonstrated computed tomography at 140 nm half-period resolution using a compact soft x-ray microscope with a high-resolution zone plate objective. The resolution of the tomogram was limited by the number of collected projections and the DOF of the zone plate objective. Higher resolution can be reached with more projections, but it requires a maximal sample size equal to the DOF for that resolution. The long exposure times needed for high-resolution compact soft x-ray microscopy make the photon economy important. The DOF of ordinary zone plates depends on the NA, which should be matched with the NA of the illumination for good photon economy. The development of extended DOF optics is therefore also of great importance, as is improving the illumination photon flux for operation at $\lambda = 2.48$ nm, which gives a larger penetration depth and shorter exposure times.

To reach higher resolution and make computed tomography of thick hydrated biological samples possible, we are presently upgrading the microscope. The source brightness will be improved with a new high power laser (diode-pumped Nd:YAG, 2 kHz, 100 mJ, <1 ns pulses). Present operation at $\lambda = 2.48$ nm is based on a zone plate condenser [6]. This condenser will be replaced with a multilayer mirror condenser, which will focus a larger solid angle of the emitted radiation onto the specimen. The option of a motorized and rotatable cryo sample stage is being implemented into the microscope. The motorized stage makes the acquisition of tilt series easier and more accurate, and the possibility to keep biological samples cryo-fixated during exposure is of great importance for reducing the effects of radiation damage [23]. With these improvements compact soft x-ray microscopy could become one of the standard tools for high-resolution computed tomography of biological specimens.

Acknowledgements

We would like to thank Sofie-Charlotte Gleber and Julia Sedlmair for providing the glass capillaries for the experiment. The financial support of the Swedish Science Research Council and the Swedish Strategic Research Foundation is gratefully acknowledged.

#107683 - $15.00 USD Received 17 Feb 2009; revised 21 Apr 2009; accepted 10 Jun 2009; published 18 Jun 2009